The magnetohydrodynamic flow past a non-conducting flat plate in the presence of a transverse magnetic field

By D. M. DIX

Department of Mechanical Engineering, Massachusetts Institute of Technology, Cambridge, Massachusetts†

(Received 20 April 1962 and in revised form 8 October 1962)

The general character of the magnetohydrodynamic flow past a non-conducting flat plate in the presence of transverse magnetic fields is analysed in some detail. The appropriate extension of the Rayleigh problem to the magnetohydrodynamic case is shown to yield solutions which correctly predict some features of the steady flow past a semi-infinite flat plate; in addition, it is shown that the knowledge of these significant features permits an easy evaluation of their magnitudes in other extensions of the Rayleigh problem. The flow past a semi-infinite flat plate is analysed by two methods. First, by linearizing the governing equations and incorporating the assumption of a low ratio of viscous to magnetic diffusivity, the results for skin friction and the normal component of magnetic field at the plate are obtained, and are shown to be useful in interpreting the character of these low conductivity flows. Secondly, the complete set of governing equations is formulated as a finite difference problem and solved numerically on a digital computer. The results obtained, in addition to demonstrating feasibility of the numerical calculations, show that the disturbance produced by the plate is no longer confined to a thin viscous layer if the ratio of viscous to magnetic diffusivity is greater than 10^{-2}, but that an appreciable Alfvén type disturbance is excited.

1. Introduction

The purpose of this communication is to present the results of a theoretical investigation of the problem stated by the title. This problem, as study of the pure fluid mechanics analogue has shown, is of fundamental importance to the flow about obstacles and at system boundaries. The paper is divided into four parts. In § 2, various extensions of the Rayleigh problem are discussed, the emphasis being placed upon the significant physical aspects of the flow and their relationship to the steady flow past a semi-infinite flat plate. In § 3, the latter problem is formulated, linearized, and solved in an approximate manner for the skin friction and the normal component of magnetic field at the plate under the assumption that the ratio of viscous to magnetic diffusivities is small. In § 4, the complete set of governing equations of the semi-infinite plate problem is formulated as a finite-difference problem and solved numerically on a digital

† Present address: Aerospace Corporation, El Segundo, California.

computer. In § 5, the results obtained are compared with the previous analytical results, and the qualitative character of the flow is emphasized.

The basic assumptions employed throughout are the usual magnetohydrodynamic ones; the fluid velocity is assumed small compared with the velocity of light and hence displacement currents are neglected; the fluid is assumed to be an incompressible, macroscopically neutral continuum with constant transport properties, and the conventional form of Ohm's Law is employed.

The following notation, unless otherwise defined, is employed:

A	magnetic vector potential, $\nabla \times (\mathbf{k}A) = \mathbf{B}$	u, v	Cartesian components of velocity $\mathbf{V}$
a	Alfvén velocity, $a = B/\sqrt{(\mu_0 \rho)}$	α	dimensionless Alfvén velocity, $\alpha = a/U$
B	magnetic intensity	δ	viscous layer thickness
D	larger of the two diffusivities, ν or $1/\mu_0 \sigma$	ϵ	ratio of diffusivities
E	electric field	ζ	vorticity, $\lvert\nabla \times \mathbf{V}\rvert$
f	skin friction	μ_0	permeability of free space
h	distance from plate to transverse boundary	ν	kinematic viscosity
J	current density	ρ	density
l	distance from leading edge to downstream boundary	σ	electrical conductivity
		Ψ	stream function; $\nabla \times (\mathbf{k}\Psi) = \mathbf{V}$

The subscripts employed are:

a	refers either to position of Alfvén wave or conditions immediately behind it	s	refers to separation distance
		$0, \infty$	refer to ambient conditions
g	refers to characteristic growth length	$1, 2$	refer to conditions upstream and downstream of Alfvén line, respectively.
H	refers to Hartmann layer		

Field quantities, with asterisks, are dimensional; otherwise they are non-dimensional.

2. The Rayleigh problem

2.1. *Introductory remarks*

In the fluid mechanics sense, the classical Rayleigh problem is that in which a thin, infinite plate is started impulsively from rest in its own plane in an unbounded viscous medium. The usefulness of such a problem is that it exhibits qualitative boundary-layer characteristics and in this respect yields insight into the behaviour of the steady, two-dimensional flow past a semi-infinite flat plate. With the introduction of electromagnetic effects, considerable latitude exists in the choice of electromagnetic properties of the plate, orientation of the applied magnetic field, form of electromagnetic boundary conditions, and excitation methods, resulting in many possible magnetohydrodynamic extensions. As it happens, the governing equations of the various extensions of fundamental

interest in the incompressible problem retain the linearity of the classical problem.

Some extensions of the problem have been considered by previous investigators. Rossow (1960) and Dix & Cooper (1960) attacked the problem of a non-conducting plate started impulsively from rest with velocity U_p^* with an applied magnetic field B_0^* perpendicular to the plate (see figure 1*a*), and Carrier &

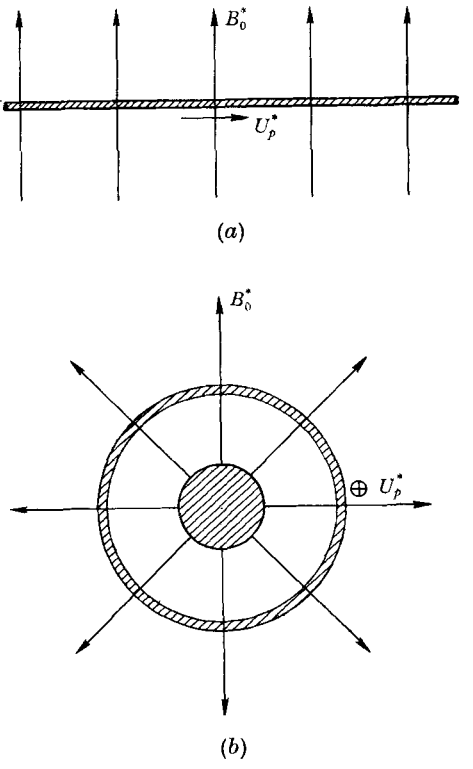

FIGURE 1. (*a*) Plane Rayleigh problem; (*b*) annular Rayleigh problem.

Greenspan (1960) the corresponding annular problem (see figure 1*b*). Chang & Yen (1959) and Ludford (1959) considered the problem of the infinitely conducting plate. It is the purpose of the following discussion to indicate how the significant features of any of the above flows, together with others which have not yet appeared in the literature,† may be obtained without recourse to elaborate analysis.

2.2. *The ultimate state*

The significant features of the flow, as obtained by previous investigators, are the formation of a viscous layer adjacent to the plate and the generation of an Alfvén wave which propagates into the fluid at its characteristic speed, a, and

† More recent work by Bryson & Rościszewski (1962), which appeared after the completion of the present work, treats various extensions of the Rayleigh problem quite thoroughly; however, it is felt that the simple physical arguments presented here are still of value in emphasizing the basic character of the flow.

diffuses. At some time after the start of the motion, the wave is clear of the viscous layer, the latter is fully developed, and the flow behind the wave is quasi-steady. The qualitative character of this flow is shown in figure 2. The relative strengths of the wave and viscous layer are determined by the ratio (ϵ) of the two diffusivities, ν and $1/\mu_0\sigma$, which is the only parameter of the problem. This flow will be referred to as the ultimate state, and it is of interest to determine the time required for it to develop and the velocity and magnetic field changes across the viscous layer and the Alfvén wave.

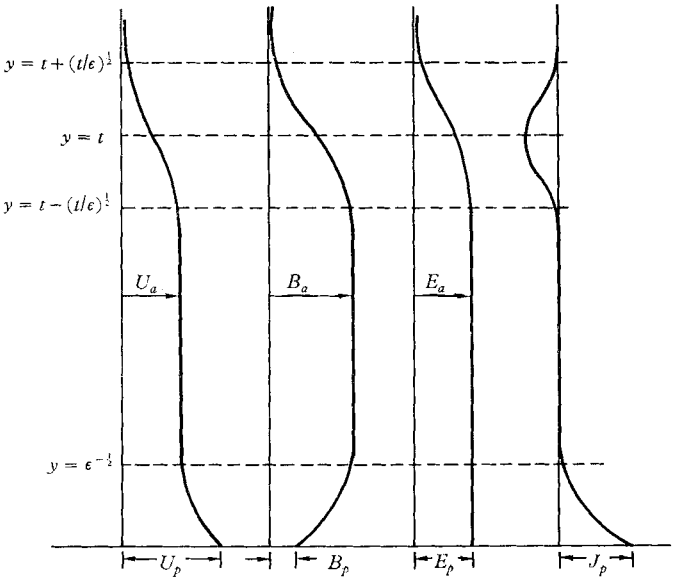

FIGURE 2. Qualitative Rayleigh profiles for $t \gg 1$.

To fix ideas, the problem considered is that in which the initial state is stationary and free of currents (other initial states may be treated easily by superposition), and there is fluid on both sides of the plate; the plate, however, may be either non-conducting or it may be a conducting plate which is insulated from the fluid, or it may be an uninsulated conducting plate. The net result of these considerations is that the initiating mechanism may either be a motion imparted to the plate, a longitudinal component of magnetic field applied at the surface of the plate, or both.

The time duration necessary for the ultimate state to be established can be derived by observing that this time must be greater than the time for the viscous layer to develop and such that the distance the wave has travelled is greater than both the width of the wave and the width of the viscous layer. In the fully developed viscous layer, the magnetic forces are equal and opposite to the viscous forces, and the inertial forces vanish. The time required for the development of this layer is therefore that required for the magnetic forces to become greater than the inertial forces, i.e. $t_v^* \sim \rho/\sigma B_0^{*2}$. The thickness of the fully developed layer is determined by the fact that the magnetic and viscous forces are equal, i.e. $\delta_H^* \sim (\rho\nu/\sigma B_0^{*2})^{\frac{1}{2}}$. The width of the Alfvén wave is given by $(Dt^*)^{\frac{1}{2}}$,

where D is the greater of the two diffusivities, ν or $1/\mu_0\sigma$. Therefore, the time at which the wave is as broad as the distance travelled is $t^*_D \sim D/a^2$, and the time at which the wave has travelled a distance equal to the thickness of the viscous layer is $t^* \sim \epsilon^{\frac{1}{2}}\rho/\sigma B_0^{*2}$. These conditions reduce to the single requirement that $t^* \gg D\mu_0\rho/B_0^{*2}$ for the ultimate state to be achieved. It is pointed out that in this sense the ultimate state is never achieved if either $\sigma \to 0$ or $B_0^* \to 0$. This is the principal difference between the ordinary Rayleigh problem and the various magnetohydrodynamic extensions.

The relations governing the relative strengths of the viscous layer and Alfvén wave are simply the statements that the change in the (longitudinal) component of magnetic field across the Hartmann layer is related to the velocity change by (using the notation of figure 2),

$$B_a^* - B_p^* = -\mu_0(\sigma\rho\nu)^{\frac{1}{2}}(U_p^* - U_a^*) \tag{2.1}$$

and that the similar relation for the Alfvén wave is

$$B_a^* = -U_a^*(\mu_0\rho)^{\frac{1}{2}}. \tag{2.2}$$

Introducing the dimensionless variables $B_a = B_a^*/B_0^*$, $U_a = U_a^*/a^*$, the solution of (2.1) and (2.2) for B_a and U_a is

$$U_a = -B_a = -\frac{1}{1+\epsilon^{\frac{1}{2}}}B_p + \frac{\epsilon^{\frac{1}{2}}}{1+\epsilon^{\frac{1}{2}}}U_p. \tag{2.3}$$

From Ohm's Law it can further be deduced that

$$E_a = -U_a = B_a. \tag{2.4}$$

It is mentioned here that the existence of E_a in a quasi-steady, current-free flow is not at all artificial as supposed by Carrier & Greenspan (1960), as it arises due to the induction effect of the Alfvén wave ($\int (dB_a/dt)\,dy \neq 0$) and of course would cause charge to accumulate at the extremes of a plane problem. It is further pointed out that providing for closed current paths, as is necessary in all magnetohydrodynamic problems, poses no difficulty in the present case, as the current induced in the viscous layer and/or the plate is exactly equal and opposite to the current in the Alfvén wave.

The effects of the various initiating mechanisms are portrayed by equations (2.3) and (2.4). If the plate is non-conducting, and given an initial velocity, then

$$U_a = -B_a = \frac{\epsilon^{\frac{1}{2}}}{1+\epsilon^{\frac{1}{2}}}U_p, \tag{2.5}$$

which is in accord with the results of previous investigators (Carrier & Greenspan 1960; Dix & Cooper 1960). If now the plate is an insulated conductor and remains stationary while an initial current is passed through the plate, then $U_p = 0$ and

$$U_a = -B_a = -\frac{1}{1+\epsilon^{\frac{1}{2}}}B_p. \tag{2.6}$$

It is pointed out in passing that if one desires to generate Alfvén waves, then the latter excitation form is obviously the optimum method, since in general ϵ will be quite small.

If $B_p = -U_p$, it is seen that no Hartmann layer develops. This is in fact the case if the plate is infinitely conducting and uninsulated (as considered by Chang & Yen 1959 and Ludford 1959), since $E_a = -U_p$.† Also this is presumably the case some authors loosely refer to as the 'field-fixed-with-respect-to-plate' case, since $E^* = -U_p^* B_0^*$.

If $B_p = \sqrt{\epsilon} U_p$, then no Alfvén wave is present; this situation can arise only with the use of an insulated conducting plate, with the conducting portion remaining stationary.

These considerations may be extended to various asymmetrical cases. For example, for fluid on one side only of an infinitely conducting plate, or an infinitely conducting pole piece, the result is the same as for the symmetrical case. For fluid on one side of an infinitely permeable magnet, the result is the same as for the non-conducting plate since $B_p = 0$. There are obviously many more extensions and modifications of this type problem, but it would be tedious and not very informative to explore them, as the essential features are no different from those previously discussed.

2.3. *Relationship to the semi-infinite plate problem*

Henceforth, the problem considered is the two-dimensional, steady flow past a non-conducting semi-infinite flat plate in the presence of an applied magnetic field transverse to the plate, with an applied electric field such that the current far upstream is zero (see figure 3). As mentioned previously, the corresponding Rayleigh problem, which in this case is that whose ultimate state is given by (2.5), may yield insight into this problem.

The analogy between the Rayleigh problem and the steady problem is made by simply replacing t^* in the former problem by x^*/U_∞^*. The qualitative character of the resulting flow is shown in figure 4. Order of magnitude considerations analogous to those applied in the Rayleigh problem yield the characteristic distances shown in the figure: (i) the characteristic growth length of the viscous layer (determined by equilibrium of inertial and magnetic forces),

$$x_g^* \sim \rho U_\infty^* / \sigma B_\infty^{*2};$$

(ii) the distance required for separation of the viscous layer and the Alfvén wave

$$x_s^* \sim \mu_0 \rho U_\infty^* D / B_\infty^{*2};$$

(iii) the fully developed thickness of the viscous layer,

$$\delta_H^* \sim (\rho \nu / \sigma)^{\frac{1}{2}} B_\infty^*;$$

(iv) the nominal position of the Alfvén 'line',

$$y_a^* \sim a x^*;$$

(v) the thickness of the Alfvén line,

$$\Delta y_a^* \sim (D x^* / U_\infty^*)^{\frac{1}{2}}.$$

† For uninsulated conducting plates, an additional restriction must be placed on the time required for the ultimate state to be achieved; it must be shorter than the magnetic diffusion time across the plate.

It is evident that this analogy is not well made if, in the steady problem, the fluid acquires a large normal velocity component or the normal component of magnetic field differs appreciably from the upstream value. The contributing magnetohydrodynamic factors are the current in the viscous layer, which tends to increase the normal component of magnetic field in the vicinity of the leading

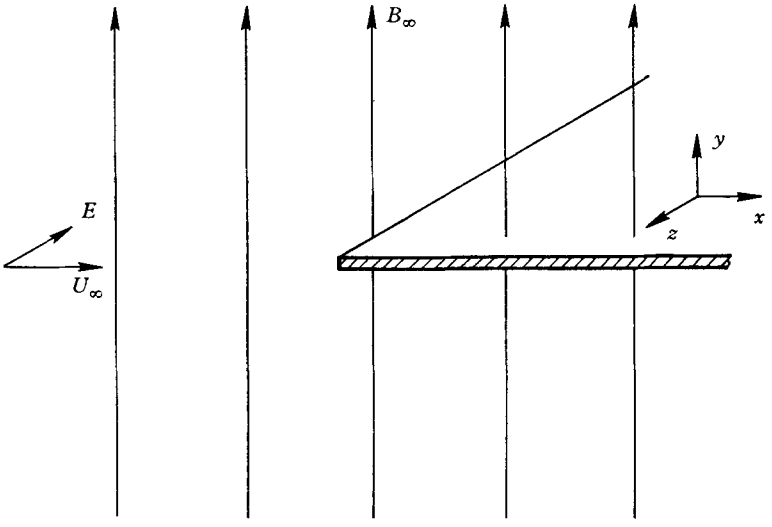

FIGURE 3. Steady two-dimensional flow past a flat plate.

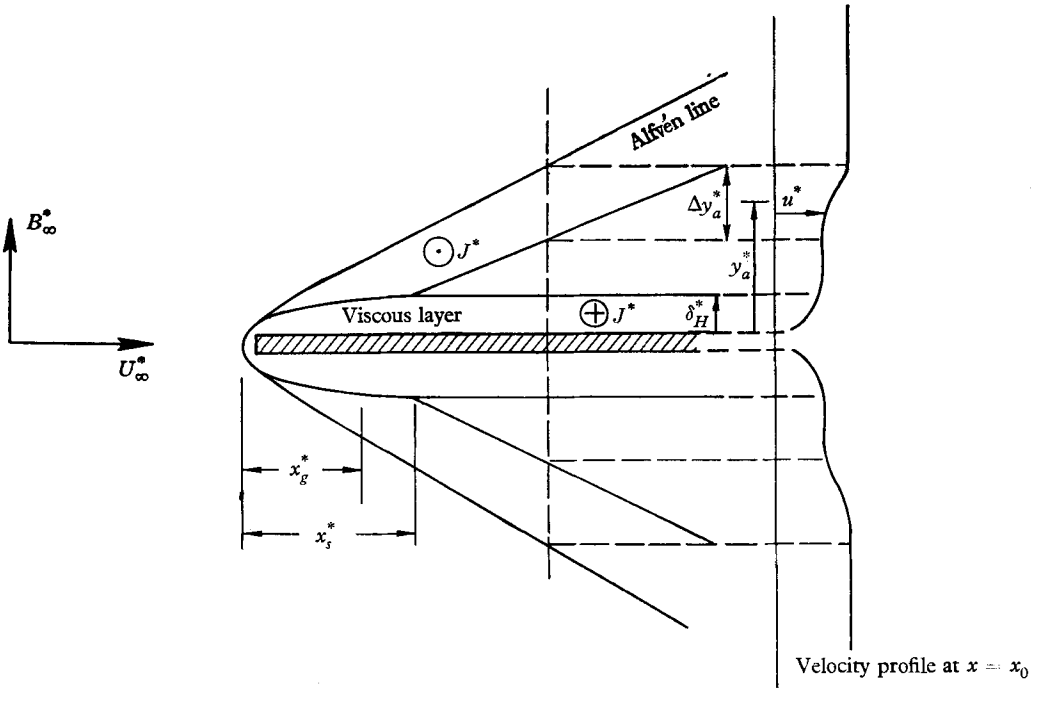

FIGURE 4. Qualitative picture of flow past a semi-infinite flat plate as constructed from the corresponding Rayleigh problem.

edge, and the oppositely directed current in the Alfvén 'line', which causes the fluid to be deflected toward the plate. It is easily shown that these effects are governed by the parameters $\sqrt{\epsilon}$ and $\alpha\sqrt{\epsilon}$; and that if either of these is not small compared to unity, the effects are not necessarily small. In this case, the analogy to the Rayleigh problem is not well taken and the flow pattern shown in figure 4 requires modification. The necessary modifications will be discussed in detail in § 5; nevertheless, it is evident at this point that the nature of such flows is such that in addition to a viscous layer adjacent to the plate, the flow is disturbed in an appreciable region away from the plate. An important physical result of the work presented here is an analysis of this effect, as it represents a significant departure from the character of the flow in the absence of a magnetic field.

It is noted that when $\sqrt{\epsilon}$ and $\alpha\sqrt{\epsilon}$ are small, which is a case of great practical interest, the analogy with the Rayleigh problem is quite well taken. Thus a viscous layer, which approaches the Hartmann layer asymptotically with the characteristic growth length x_y^*, is expected.

3. The linearized semi-infinite flat-plate problem

3.1. *Formulation of the general problem*

The more interesting problem of steady flow past a semi-infinite flat plate as shown in figure 3 is governed by the Navier–Stokes equations with the Lorentz force included and Maxwell's equations. These equations, appropriate to two dimensions, can be obtained in a convenient form by rendering them dimensionless (employing ν/U_∞, U_∞, and B_∞ as the characteristic length, velocity, and field strength, respectively) and introducing the stream function and magnetic vector potential. The governing equations then become:

$$\nabla^4\Psi + \Psi_x\nabla^2\Psi_y - \Psi_y\nabla^2\Psi_x = \alpha^2(A_x\nabla^2 A_y - A_y\nabla^2 A_x), \tag{3.1}$$

$$\nabla^2 A = -\epsilon(\Psi_x A_y - \Psi_y A_x - 1). \tag{3.2}$$

The boundary conditions are $\Psi = \Psi_y = A_y = 0$ at $y = 0$, $x > 0$; $\Psi_x \to 0$, $A_x \to -1$, $A_y \to 0$, $\Psi_y \to -1$ as $x \to -\infty$, and further that Ψ and A are reasonably well behaved as $y \to \pm\infty$ and as $x \to +\infty$. This is the complete mathematical formulation of the problem; as the equations are non-linear they offer no practical hope of analytical solution.

3.2. *The linearized problem*

It has been found both in the pure fluid mechanics case and in some magnetohydrodynamic problems (Greenspan & Carrier 1959) that linearization of the governing equations allows qualitatively useful results to be obtained. Following the usual procedure for linearization, the perturbation potentials Ψ' and A' are defined by

$$\Psi = y + \Psi', \tag{3.3}$$

$$A = A' - x, \tag{3.4}$$

and are assumed negligible in the second order. On a physical basis, the assumption that Ψ' is small is obviously not valid near the plate; similarly, the assumption that A' is small can only be justified for small ϵ. However, these deficiencies

are certainly no greater than in the pure fluid mechanics case so that qualitatively useful results may be expected.

Making the substitutions (3.3) and (3.4) into (3.1) and (3.2) and neglecting terms of second order in the primed quantities yields

$$\nabla^4\Psi' - \nabla^2\Psi'_x = \alpha^2\nabla^2 A'_y, \tag{3.5}$$

$$\nabla^2 A' = \epsilon(A'_x - \Psi'_y). \tag{3.6}$$

The corresponding boundary conditions are $\Psi' = A'_y = 0$, $\Psi'_y = -1$ at $y = 0$, $x > 0$; $\Psi'_x = A'_x = A'_y = \Psi'_y \to 0$ as $x \to -\infty$, and reasonable behaviour of Ψ' and A' as $y \to \pm\infty$ and as $x \to +\infty$. Unfortunately, because of the mutual coupling of the equations, the analysis of this problem is exceedingly complex. It is therefore convenient to introduce the further assumption that the rate of change in the normal component of magnetic field (B_y) in the y direction is much less than the rate of change of the longitudinal component of velocity (u) in the y-direction ($A_{xy} \ll \Psi_{yy}$). It can readily be shown that near the plate, where the right side of (3.6) is largest in magnitude, this is a valid assumption for ϵ not large. In the region away from the plate, the assumption cannot be justified, but for small ϵ, the contribution of both terms is small. Introducing this assumption into (3.5) and (3.6) and rearranging, the governing equations become

$$\nabla^4\Psi' - \nabla^2\Psi'_x = \epsilon\alpha^2\Psi'_{yy}, \tag{3.7}$$

$$\nabla^2 A' = \epsilon(A'_x - \Psi'_y). \tag{3.8}$$

It is evident that the preceding equations constitute a relatively simple set, as the stream function is now uncoupled. The significance of the parameters ϵ and $\epsilon\alpha^2$ as determining, respectively, the magnitude of the induced magnetic field caused by the flow and the effect of the applied magnetic field on the flow, is clearly shown.

The solution of the set of equations (3.7) and (3.8) with the associated boundary conditions is still not trivial. Briefly, the procedure consists of applying Fourier transforms in x and y to the equations and boundary conditions, treating the skin friction at the plate ($\Psi'_{yy}(y \to 0+)$) as unknown; obtaining the inverse transform in y; determining $\Psi'_{yy}(y \to 0+)$ in an approximate manner, utilizing the Weiner–Hopf technique; and, finally, obtaining the inverse transforms in x for the normal component of magnetic field at the plate. The entire procedure is similar to that of Greenspan & Carrier (1959) and hence need not be presented here. The only point which merits mention here is the approximation employed in determining $\Psi'_{yy}(y \to 0+)$. Following the first two steps mentioned above, and applying the boundary conditions at the plate yields an equation of the conventional Weiner–Hopf form, in which appears a function

$$\bar{K}(p) = \frac{1}{|N_1| + |N_2|}, \tag{3.9}$$

where $$N_1^2 = p^2 + \tfrac{1}{2}ip + \tfrac{1}{2}\epsilon\alpha^2 \pm \tfrac{1}{2}[(4\epsilon\alpha^2 - 1)p^2 + 2\epsilon\alpha^2 ip + \epsilon^2\alpha^4]^{\frac{1}{2}},$$

and p is the Fourier-transform variable in x.

To obtain a solution it is necessary to decompose this function into a product of two functions, one being analytic in the upper half plane and one being analytic in the lower half plane. In order to obtain relatively simple results it is necessary to approximate the function $\bar{K}(p)$. To this end, if $\epsilon\alpha^2 \ll 1$, N_1 and N_2 in (3.9) can be approximated by

$$N_1^2 \doteq p^2 + ip + \epsilon\alpha^2,$$

$$N_2^2 \doteq p^2,$$

so that $\bar{K}$ becomes

$$\bar{K}(p) \doteq \{|p| + |p^2 + ip + \epsilon\alpha^2|^{\frac{1}{2}}\}^{-1}. \tag{3.10}$$

The basic approximation technique is now to replace $K(x)$ by another function $D(x)$ which is easily factored, but retains the essential features of the flow. Carrier (1959) has demonstrated that by requiring D to possess the same singularity and the same area and first moment as K, a very good approximation is obtained. If the contribution of $\epsilon\alpha^2$ to the first moment of K is neglected then the transform of the appropriate approximate function is

$$\bar{D}(p) = \left(2p + \frac{i}{4}\right)^{-\frac{1}{2}} (p - i\epsilon\alpha^2)^{-\frac{1}{2}} \doteq \bar{K}(p), \tag{3.11}$$

which can be decomposed by inspection. The solution then proceeds as mentioned previously.

3.3. *Discussion of results of linearized problem*

Following the procedure outlined in the previous section results in solutions for the skin friction and normal component of magnetic field at the plate that are given by

$$\Psi'_{yy}(y = 0+, x > 0) = \frac{1}{(\pi x)^{\frac{1}{2}}} e^{-\epsilon\alpha^2 x} + (\epsilon\alpha^2)^{\frac{1}{2}} \operatorname{erf}(\epsilon\alpha^2 x)^{\frac{1}{2}}, \tag{3.12}$$

$$-A'_x(y = 0, x > 0) = \frac{1}{\pi} \int_0^{\epsilon\alpha^2} \frac{(r+\epsilon)^{\frac{1}{2}} - r^{\frac{1}{2}}}{(\epsilon\alpha^2 - r)^{\frac{1}{2}} r^{\frac{1}{2}}} e^{-rx}\, dr. \tag{3.13}$$

The assumptions made during the course of the solution restrict the validity of these results to those cases where $\epsilon \ll 1$, $\epsilon\alpha^2 \ll 1$, $x \gg 1$. The relation (3.13) is plotted in figure 5.

The physical basis of (3.12) is easily deduced. The first term is merely the classical result of the pure fluid mechanics case multiplied by a decay factor; the second term is the skin friction attributed to a fully developed Hartmann layer (i.e. the inertial forces vanish) multiplied by a growth factor. It is worth mentioning that this relation may be obtained directly from the results of the corresponding Rayleigh problem for $\epsilon \ll 1$ if t^* is replaced by x^*/U_∞^*; hence the characteristic growth of the boundary layer $x_g = 1/\epsilon\alpha^2$ is exactly that obtained from the previous analogy (§ 2.3).

From figure 5, it is seen that the maximum perturbation in the normal component of magnetic field at the plate occurs at the leading edge, and is of the order $\epsilon^{\frac{1}{2}}$. This result is physically reasonable as more distortion is expected at higher conductivities (higher ϵ). Also, as α is increased, the fully developed layer

is thinner, and is arrived at in a shorter distance; this indicates a smaller disturbance to the flow and hence it is expected that the magnetic field distortion is decreased, which is indeed apparent in figure 5.

It was previously pointed out that, for the case of small ϵ, the greatest deficiency in the linearization process was the replacement of u by $1-u'$, with u' assumed small. From equations (3.1) and (3.2), it is seen that the major effect of this linearization is in the inertial terms of equation (3.1), just as in the fluid mechanics case. If these inertial terms are written in terms of the vorticity, i.e. $u\zeta_x + v\zeta_y$, it is easily seen that the average values of u and v selected in the

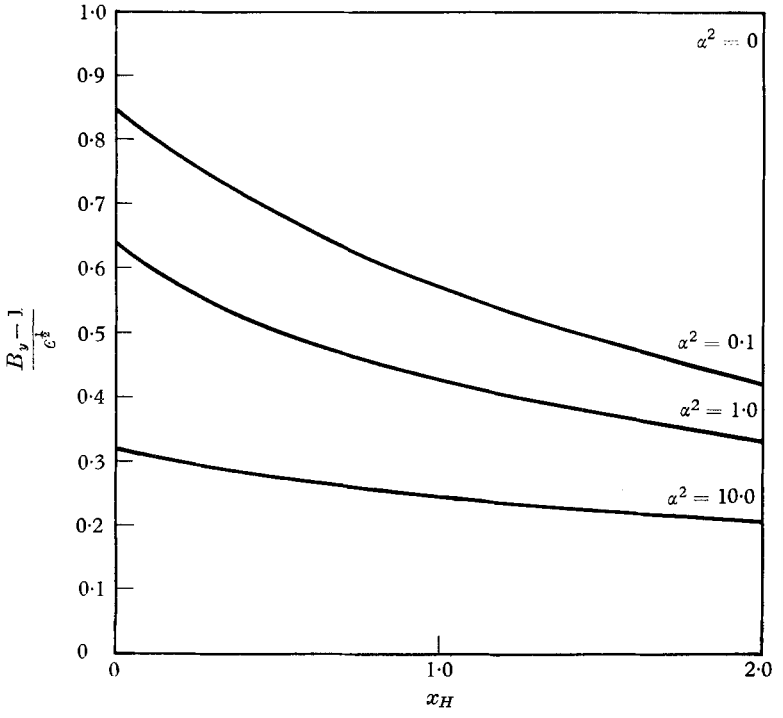

FIGURE 5. Linearized solution for normal component of magnetic field at plate.

linearization process govern the distribution of vorticity. It is obvious that the value $u = 1$ is a gross overestimate; in the fluid mechanics case, it has been found that selecting average values of $u = 0{\cdot}335$, $v = 0$ distributes the vorticity in such a manner that the skin friction at the plate is identical to that obtained from the classical Blasius solution. It can therefore be expected that some improvement of the results obtained in the present case can be made by a more judicious selection of this average value. For the present we shall denote this value by K; the results analogous to (3.12) and (3.13) are then

$$\Psi''_{yy}(y = 0+, x > 0) = (\pi x/K)^{-\frac{1}{2}} e^{-\epsilon\alpha^2 x/K} + (\epsilon\alpha^2)^{\frac{1}{2}} \operatorname{erf}(\epsilon\alpha^2 x/K)^{\frac{1}{2}}, \tag{3.14}$$

$$-A'_x(y = 0, x > 0) = \frac{1}{\pi\sqrt{K}} \int_0^{\epsilon\alpha^2/K} \frac{(r+\epsilon)^{\frac{1}{2}} - r^{\frac{1}{2}}}{(\epsilon\alpha^2/K - r)^{\frac{1}{2}} r^{\frac{1}{2}}} e^{-rx}\, dr. \tag{3.15}$$

Use of these results will be made in § 5.

4. Numerical solution of the complete problem

4.1. *Formulation of the differential problem*

The results of §§ 2 and 3 yield a great deal of insight into the semi-infinite plate problem for small ϵ; to obtain more quantitative information for this case, and to treat the case of ϵ not small, the considerably more elaborate technique of numerically solving the complete set of equations as given by (3.1) and (3.2) is employed. This requires the complex and tedious procedure of formulating a finite difference problem and developing and programming a solution technique suitable for digital computation. Only the salient features of this process will be discussed here. It must be pointed out, however, that the purpose of this numerical work is more to determine the character of the flow rather than to obtain a high degree of numerical accuracy.

Equations (3.1) and (3.2) and the associated boundary conditions can be properly formulated as a boundary-value problem. To circumvent difficulties associated with non-linear algebraic equations, the vorticity, ζ, is introduced into (3.1) and (3.2) as an auxiliary variable, and the result rearranged slightly to yield:

$$\nabla^2\zeta - (\Psi_x\zeta_y - \Psi_y\zeta_x) = \epsilon\alpha^2[-A_y(\Psi_x A_y - \Psi_y A_x)_x + A_x(\Psi_x A_y - \Psi_y A_x)_y], \quad (4.1)$$

$$\nabla^2\Psi = -\zeta, \quad (4.2)$$

$$\nabla^2 A = -\epsilon(\Psi_x A_y - \Psi_y A_x - 1). \quad (4.3)$$

In order to incorporate boundaries located at finite positions, the model selected here can be visualized as the flow past a flat plate which is a member of an infinite two-dimensional cascade (figure 6). The boundaries parallel to the free-stream flow are then selected as the two lines of symmetry; one along the plate and one along the centre line of a channel. The corresponding boundary conditions become $\Psi = h$, $\zeta = A_y = 0$ at $y = h$; $\Psi = \zeta = A_y = 0$ at $y = 0$, $x_u < x < 0$; $\Psi_y = \Psi = A_y = 0, \zeta = -\Psi_{yy}$ at $y = 0, 0 < x < l$. The conditions at the upstream boundary are assumed to be that of uniform flow; i.e. $\Psi = y$, $\zeta = A = 0$ at $x = x_u$. The conditions of the fluid quantities at the downstream boundary are taken to be those of fully developed Hartmann flow of half-channel width h; i.e. $\Psi = \Psi_H$; $\zeta = \zeta_H$ at $x = l$; the condition on the magnetic vector potential is taken as $A_{xx} = 0$. In a physical sense, these latter boundary conditions require fluid sources and sinks and electrical currents in the region outside the imposed boundaries. The contributions of these sources and sinks are small by virtue of the boundary conditions selected; evaluations of their contributions can be made by systematically repositioning the boundaries and will be discussed subsequently. It is further mentioned that weaker conditions (for example, conditions on various derivatives) have been attempted, but the difficulty in obtaining convergence of the numerical technique employed prohibited their use.

The following two sections are devoted to a discussion of the more interesting details of formulating and solving the finite difference problem; these may be omitted with no loss in continuity.

4.2. *The finite difference problem*

The finite difference net employed here is a variably spaced rectangular net, chosen so that the net spacing may be made small near the plate where fluid quantities vary rapidly. The finite difference equations are obtained from (4.1), (4.2), and (4.3) by replacing the derivatives by appropriate finite difference approximations. These approximations are obtained by expanding the function at a point in a Taylor's series; e.g.

$$\Psi'_{i+1,j} = \Psi'_{i,j} + h_{y1}\left(\frac{\partial \Psi'}{\partial y}\right)_{i,j} + \frac{h_{y1}^2}{2}\left(\frac{\partial^2 \Psi'}{\partial y^2}\right)_{i,j} + \ldots. \tag{4.4}$$

In the present case only the first three terms of the series are retained; writing a similar expression for $\Psi'_{i-1,j}$ yields a set of equations which may be solved for

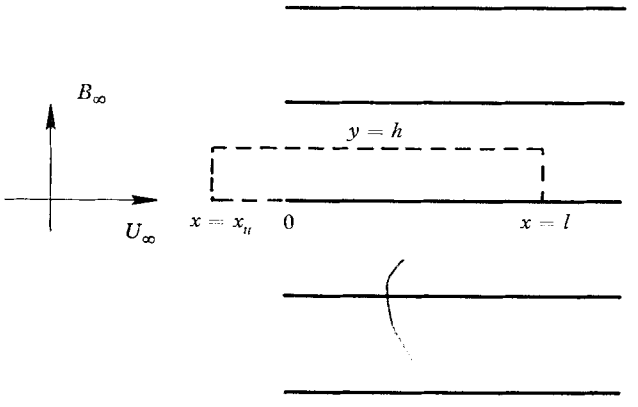

FIGURE 6. Two-dimensional cascade of plates showing domain of consideration.

$(\partial \Psi'/\partial y)_{i,j}$ and $(\partial^2 \Psi'/\partial y^2)_{i,j}$. A similar procedure may be applied for the x-derivatives, while the cross-derivative is obtained from the substitution

$$\partial^2 \Psi'/\partial x \partial y = \partial/\partial x[\partial \Psi'/\partial y].$$

It may be shown that the truncation error in the approximations so obtained is of order h in the even derivatives and of the order h^2 in the odd derivatives.

The following procedure, consistent with second-order equations, regarding the boundary points at which the finite difference equations may be written, is employed. If a function is prescribed at a boundary, then the finite difference equation is not written at those boundary points; if, however, a normal derivative is prescribed, then the finite difference equation is written at those boundary points. The latter process introduces fictitious points exterior to the boundary; the values of the relevant functions at these points are found from writing the finite difference boundary conditions. Finally, the values at the fictitious points are eliminated with these relations, resulting in a simultaneous set of equations for each of the functions Ψ', ζ, A which involve only values at points located at or within the physical boundaries.

The leading edge of the plate constitutes a minor difficulty, as the vorticity is singular there. However, numerical results obtained by successively reducing

the net spacing have shown that the error encountered due to this singularity can be confined to an arbitrarily small region surrounding the leading edge, and hence is of no practical consequence.

4.3. *Solution technique*

A direct simultaneous solution of the finite difference equations for Ψ', ζ and A is not feasible. The general method employed here is one of multiple iteration, in which the equations for Ψ', ζ, and A are solved separately, assuming that the other two dependent variables are known: thus it involves only linear algebraic equations. The specific procedure consists of the following seven steps:

(1) Estimate the unknown values of ζ and A at the net points.

(2) Solve the stream-function equations (4.2), using current values of ζ and A.

(3) Calculate the vorticity at the plate from a weighted sum of the current value and that computed from the Ψ' values obtained in (2).

(4) Solve the vorticity equations (4.1), using current Ψ' and A values and the values of ζ at the plate calculated in (3).

(5) Repeat steps (2)–(4) until satisfactory agreement is obtained between two successive sets of values of ζ.

(6) Solve the magnetic potential equations (4.3) using current values of ζ and Ψ'.

(7) Repeat steps (2)–(6) until satisfactory agreement between two successive sets of values of A is obtained.

The direct, simultaneous solution of the separate sets of equations for Ψ', ζ and A, required in steps (2), (4) and (6) again is not feasible, and hence another iterative scheme is employed. This process, which is essentially a block relaxation technique, is described as follows. Beginning at the row of net points nearest the plate at which the values of the relevant function are unknown, the set of equations formed by the finite difference equations of every relevant point in the row is solved simultaneously for the values of the variable at the points in the row, holding constant the values at points not in the row. These values then replace the original values and the process is repeated for every row in the net, moving from the plate outward, to complete one iteration. This iteration process is repeated until satisfactory agreement between two successive sets of values of the dependent variable is obtained. It is worth mentioning that the more usual procedures of iteration by single or total steps fail to converge in the present case, due to the fact that, for practical values of net spacing in the region away from the plate, the matrix resulting from the application of the finite difference form of (4.1) is not positive definite.

The above procedure was programmed for, and solution carried out on the IBM 709; the following details of the numerical solution procedure merit additional mention. First, in all cases reported here, the initial estimates of A were those corresponding to a uniform magnetic field; thus the completion of step (5) in the solution procedure yields the solution for no magnetic field distortion (which will henceforth be referred to as Hartmann flow). Secondly, the weighting factor introduced into step (3) of the solution is necessary due to the fact that as the magnitude of the stream function is very small near the plate, the values are

very sensitive to the current value of ζ. Numerical computations have shown that the weighting factor must be such that less than 20 % of the value computed from the new Ψ values is used. Thirdly, the net spacing employed is of the general form of $\Delta x_n = ae^{-bn}$ where a and b are determined experimentally. Exceptions to this form occur in the x spacing very near to and very far from the leading edge of the plate, where equal spacing is employed in both regions. Fourthly, the solution tends to oscillate due to truncation error; hence if any single net spacing is very large, a large oscillation is introduced into the solution. With suitable caution in the selection of net spacing, this oscillatory character may be suppressed; in the cases reported here, the maximum oscillation in vorticity is 1 % or less of the fully developed Hartmann flow value. Fifthly, the criterion employed for obtaining convergence is based on a maximum allowable percentage change between two successive sets of values; e.g. if

$$\frac{|\Psi^{(n+1)} - \Psi^{(n)}|}{\Psi^{(n)}} < T,$$

then convergence is assumed satisfactory. In the case of vorticity, this criterion is modified to

$$\left|\frac{\zeta^{(n+1)} - \zeta^{(n)}}{\zeta^{(n)} + K}\right| < T,$$

where K is a number much smaller than the peak value of vorticity; this avoids requiring excessive accuracy at points where the magnitude of the vorticity is so small as to be negligible. The tolerances employed in all cases is 0·005 for ζ and 0·003 for Ψ. It was found by decreasing these tolerances that the only quantities which changed by a percentage equivalent to that indicated by the tolerances were the vorticity and stream-function values at the plate near the downstream boundary. In other regions, changes in significant results were confined to the fourth or fifth significant figure. The convergence tolerances employed for A are governed by the same criteria and ranged from 3×10^{-5} to 4×10^{-7}, the small values being necessitated by small changes in A.

4.4. *Results*

All cases investigated here had as their origin one of two basic Hartmann (no magnetic field distortion) flows. The values of the parameter $\epsilon\alpha^2$, which completely characterizes this type of flow, are 10^{-2} and 10^{-3}. These values result in Hartmann layer thicknesses ($\delta_H = (\epsilon\alpha^2)^{-\frac{1}{2}}$) of 10 and 31·6, respectively, and characteristic growth lengths ($x_g = 1/\epsilon\alpha^2$) of 10^2 and 10^3, respectively. The boundary placement arrangements corresponding to these basic flows are shown in figure 7. These arrangements will be referred to as numbers 1, 2, 3 and 4, corresponding to those for $\epsilon\alpha^2 = 10^{-3}$, $\epsilon\alpha^2 = 10^{-2}$, $\epsilon\alpha^2 = 10^{-3}$ with the transverse boundary placed further from the plate, and $\epsilon\alpha^2 = 10^{-2}$ with the downstream boundary placed closer to the leading edge, respectively. The significant features of these arrangements are characterized by two length ratios, which indicate the magnitude of channelling effects and the relative importance of the downstream boundary position, respectively; the ratio of the Hartmann thickness, δ_H, to the half-channel width, h, and the ratio of the distance from the leading edge to the downstream boundary, l, to the characteristic growth length of the Hartmann

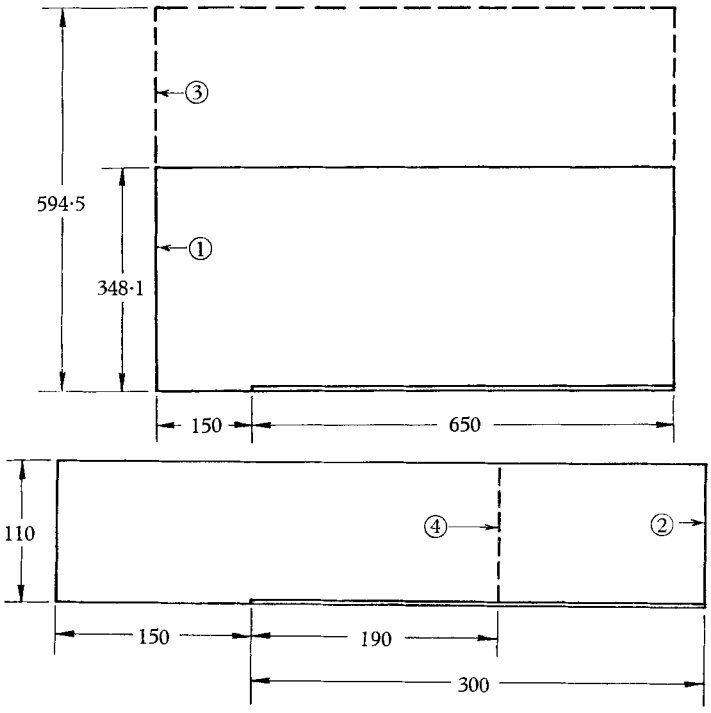

FIGURE 7. Boundary placement arrangements for $\epsilon\alpha^2 = 10^{-3}$ (top) and $\epsilon\alpha^2 = 10^{-2}$ (bottom). Distances shown are based on Reynolds number.

Arrangement	δ_H/h	l/x_g
1	$\sim 0{\cdot}1$	0·65
2	$\sim 0{\cdot}1$	3·0
3	$\sim 0{\cdot}05$	0·65
4	$\sim 0{\cdot}1$	1·90

layer, x_g. The values of these ratios for the four arrangements are also summarized in figure 7.

Each case for which results are presented here will be referred to by the notation case N–M, where N will refer to the boundary placement arrangement and M will refer, in general, to increasing values of ϵ. Numerical results were obtained, and some form of results are presented for the ten cases listed in the following table:

Case	$\epsilon\alpha^2$	ϵ	Remarks
1–1	10^{-3}	0	Hartmann type flow
1–2	10^{-3}	10^{-3}	—
1–3	10^{-3}	10^{-2}	—
1–4	10^{-3}	10^{-1}	—
2–1	10^{-2}	0	Hartmann type flow
2–2	10^{-2}	10^{-1}	—
3–1	10^{-3}	0	Transverse boundary effect, Hartmann type flow
3–2	10^{-3}	10^{-1}	Transverse boundary effect
4–1	10^{-2}	0	Downstream boundary effect, Hartmann type flow
4–2	10^{-2}	10^{-1}	Downstream boundary effect

The results for the various cases are presented in selected graphical and tabular form and are discussed in the following section.

5. Discussion of results

5.1. *Hartmann flow*

In order to compare the skin friction obtained for the Hartmann type flows (cases 1–1, 2–1, 3–1 and 4–1) with that obtained from the linearized solution of § 3, it is necessary to evaluate the effects of the finite position of the transverse and downstream boundaries on the numerical results. The effect of the transverse boundary on the numerical results was approximately eliminated by dividing the actual skin friction obtained at a given x-co-ordinate by the dimensionless

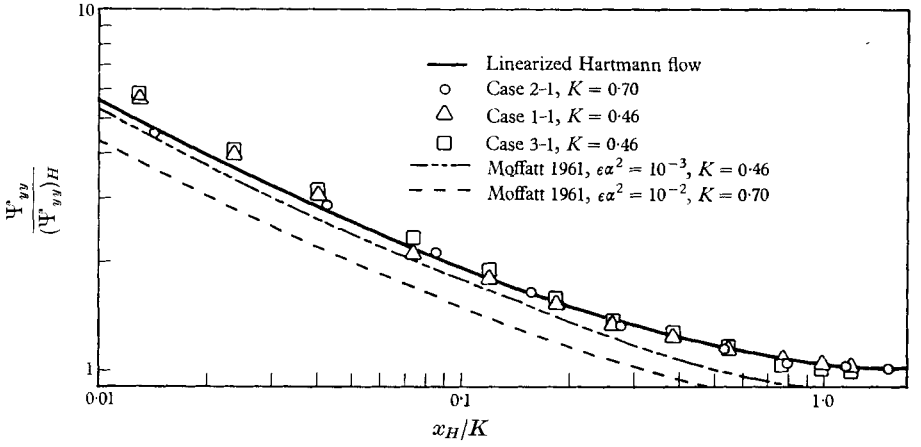

FIGURE 8. Comparison of skin friction as obtained from numerical solution with that of linearized solution.

velocity at the transverse boundary at the same x-co-ordinate; the validity of this procedure is demonstrated by comparison of the results of cases 1–1 and 3–1 in figure 8. The location of the downstream boundary has no appreciable effect (less than 0·5 %) in the results of cases 2–1 and 4–1, although there is an appreciable difference in the ratio l/x_g (3·0 as compared to 1·9, respectively). In cases 1–1 and 3–1, $l/x_g = 0{\cdot}65$ and it is expected that the downstream boundary effect is somewhat, but not significantly, greater than in the preceding cases. Finally, the selection of the average value of the longitudinal component of velocity to be used in the linearized solution the factor K in equation (3.4) was made on the basis of obtaining a reasonable correlation with the numerical results, and is therefore somewhat arbitrary.

The comparison of the numerical results with the linearized solution, shown in figure 8, possesses two significant features. First, although the correlation obtained using a single value of K for any given case is relatively good, it is not exact, and it must be concluded that the functional form of the linearized solution is not exactly correct. Secondly, as the value of the interaction parameter, $\epsilon\alpha^2$, increases, the appropriate value of the factor K increases. This can be interpreted on physical grounds for as the interaction parameter increases, the viscous layer becomes thinner and hence it is expected that the appropriate average velocity employed in the linearized solution would increase.

The primary usefulness of the above results, apart from yielding insight into the general behaviour of the flow and the significant parameter involved, is as

a verification of other boundary layer calculations. For example, Moffatt (1961), employing integral methods with similar velocity profiles, obtains for the skin friction:

$$\Psi_{yy} = \frac{0{\cdot}817(\epsilon\alpha^2)^{\frac{1}{2}}}{(1-e^{-5x_H})^{\frac{1}{2}}} \quad \text{at} \quad y = 0.$$

This relation is also plotted in figure 8; it is seen that the correlation with the numerical results obtained becomes poorer as the parameter $\epsilon\alpha^2$ is increased. This indicates that the assumption of similar velocity profiles needs modification if the accuracy of the method is to be improved.

	Skin friction, $(-\xi)_{y=0}$					
Case / x	1–1	1–2	1–3	1–4	3–1	3–2
0	0·451	0·451	0·449	0·445	0·445	0·437
1	0·373	0·374	0·372	0·369	0·368	0·362
3	0·265	0·265	0·264	0·261	0·261	0·257
6	0·184	0·185	0·184	0·182	0·182	0·179
11	0·132	0·132	0·132	0·131	0·130	0·128
19	0·0992	0·0991	0·0988	0·0983	0·973	0·961
34	0·0749	0·0748	0·0746	0·0744	0·732	0·726
55·1	0·0603	0·0600	0·0599	0·0600	0·585	0·583
83·9	0·0509	0·0507	0·0506	0·0509	0·491	0·492
123·5	0·0448	0·0447	0·0445	0·0449	0·430	0·433
178	0·0408	0·0408	0·0405	0·0409	0·389	0·392
253	0·0384	0·0386	0·0380	0·0382	0·366	0·367
357	0·0373	0·0373	0·0366	0·0363	0·348	0·344
454	0·0358	0·0361	0·0355	0·0360	0·339	0·248
552	0·0345	0·0344	0·0344	0·0364	0·321	0·357
650	0·0348*	0·0348*	0·0348*	0·0348*	0·332*	0·332*

	Skin friction, $(-\xi)_{y=0}$			
Case / x	2–1	2–2	4–1	4–2
0	0·773	0·748	0·773	0·748
1	0·466	0·451	0·466	0·451
3	0·296	0·288	0·296	0·288
6	0·218	0·213	0·218	0·213
11	0·170	0·168	0·170	0·168
19	0·140	0·140	0·140	0·140
34	0·121	0·122	0·121	0·122
55·1	0·113	0·113	0·113	0·113
80	0·110	0·109	0·109	0·109
105	0·109	0·107	0·109	0·108
131	0·109	0·107	0·109	0·108
159	0·109	0·107	0·110	0·110
190	0·109	0·107	0·110*	0·110*
224	0·109	0·107		
261	0·109	0·108		
300	0·110*	0·110*		

* Denotes prescribed boundary value.

TABLE 1. Effect on skin friction of increasing parameter ϵ.

5.2. *Significant features of the numerical results for the complete flow*

To interpret the numerical results fully, it is necessary not only to deduce the basic character of the flow, but also to evaluate boundary effects. The numerical results are presented and the significant features of the basic flow are discussed in the following paragraphs. Further interpretation of these results, as well as a discussion of boundary effects (apart from the observation that the influence of the boundaries is to resist changes from the Hartmann type flow without altering the basic character of the results) is presented in § 5.3.

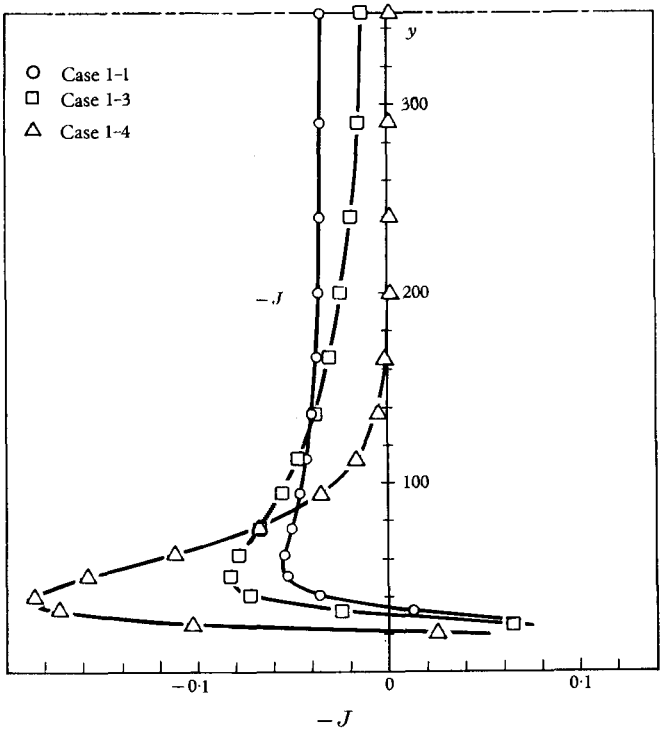

FIGURE 9. Current density profiles for cases 1–1, 1–3 and 1–4; $x = 83{\cdot}9$.

The Alfvén-wave character of the flow external to the viscous layer is most easily observed in the current density profiles shown in figures 9–11. As ϵ is increased with $\epsilon\alpha^2$ fixed), the current density becomes more concentrated, resulting in the expected maxima in the profiles. The maximum magnitudes of this effect are shown in table 2. The correlation of the location of the maxima of these profiles with that of the Alfvén line originating at $x = 0$, $y = \delta_H$, is shown in figures 12–14; as expected, the better correlations occur for the maximum value of $\epsilon = 0{\cdot}1$ employed (figures 13 and 14). The poor correlation for case 1–3 is attributed to the fact that magnetohydrodynamic interaction is not sufficient to overcome the potential flow effects created by the displacement thickness of the viscous layer. This conclusion is supported by the velocity profile shown in figure 10 for case 1–3. The lines where the current density outside the viscous

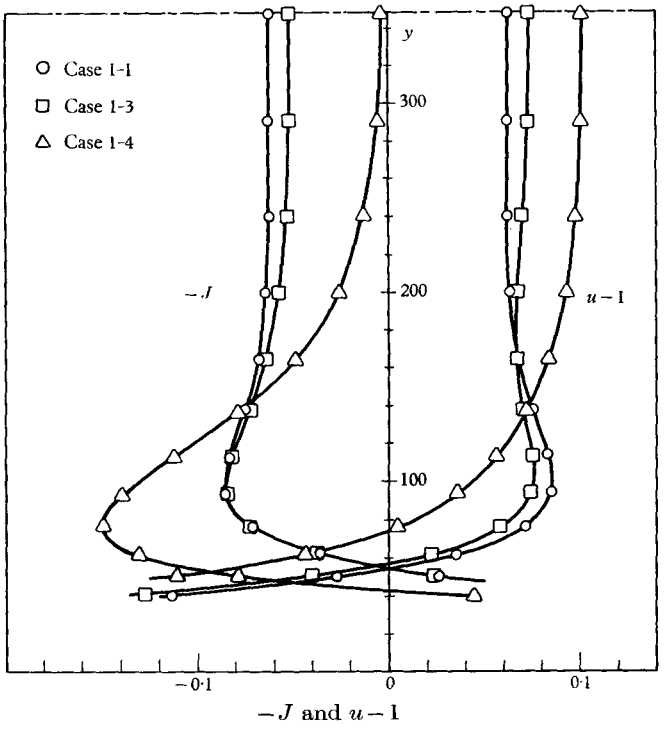

FIGURE 10. Current density and velocity profiles for cases 1–1, 1–3 and 1–4; $x = 357$.

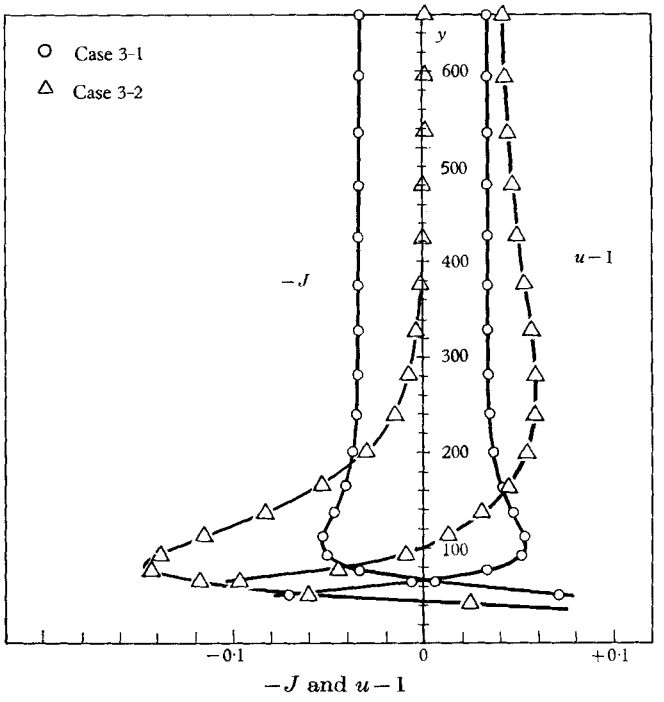

FIGURE 11. Current density and velocity profiles for cases 3–1 and 3–2; $x = 357$. Note potential flow characteristics of velocity profile for case 3–2.

layer becomes 80 % of the maximum value, also plotted in figures 13 and 14, provide a measure of the width of the Alfvén region. It can easily be shown that the width of this region increases as $\sqrt{x}$, and that the ratio of this width to the distance to the origin is of the order $1/\sqrt{\epsilon}$. This region will subsequently be referred to as the Alfvén line.

Case	x	$-J_{\max}$	$-J_H$
1–3	83·9	0·084	0·050
1–4	83·9	0·188	0·020
3–2	83·9	0·200	0·020
2–2	19	0·140	0·055

TABLE 2. Maximum magnitudes of concentration of current density.

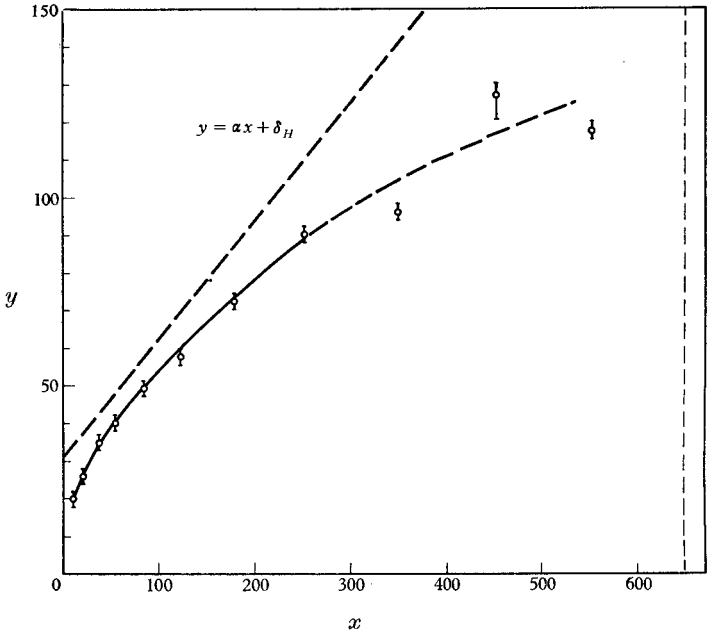

FIGURE 12. Location of maximum positive current, case 1–3: vertical lines at points are estimated uncertainty in location. Broken line on right indicates downstream boundary position.

The longitudinal velocity profiles shown in figures 10 and 11 also exhibit the presence of the Alfvén line; for, as ϵ is increased, the velocity between the Alfvén line and the plate decreases, with a corresponding increase in velocity between the Alfvén line and the transverse boundary. The maximum magnitudes of this effect are summarized in table 3. The percentage changes are the changes in velocity from the corresponding Hartmann flow values referred to the free-stream velocity. It is seen that this effect does not become appreciable until the parameter $\epsilon = 10^{-2}$ and, in the cases investigated, the maximum effect is a 9·2 % decrease (from the Hartmann flow values) in velocity near the plate and a 2·5 %

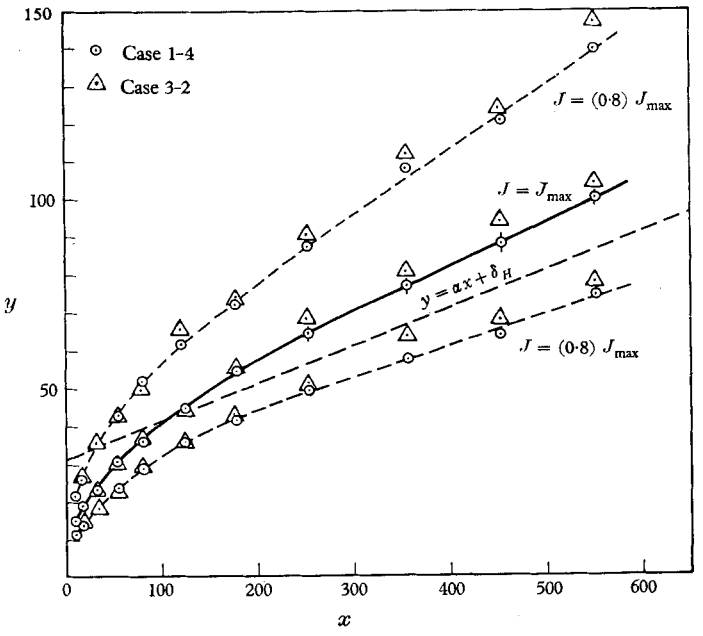

FIGURE 13. Location of maximum positive current, cases 1–4, 3–2: vertical lines at points for case 1–4 are estimated uncertainty in location of maxima. Downstream boundary position is at far right.

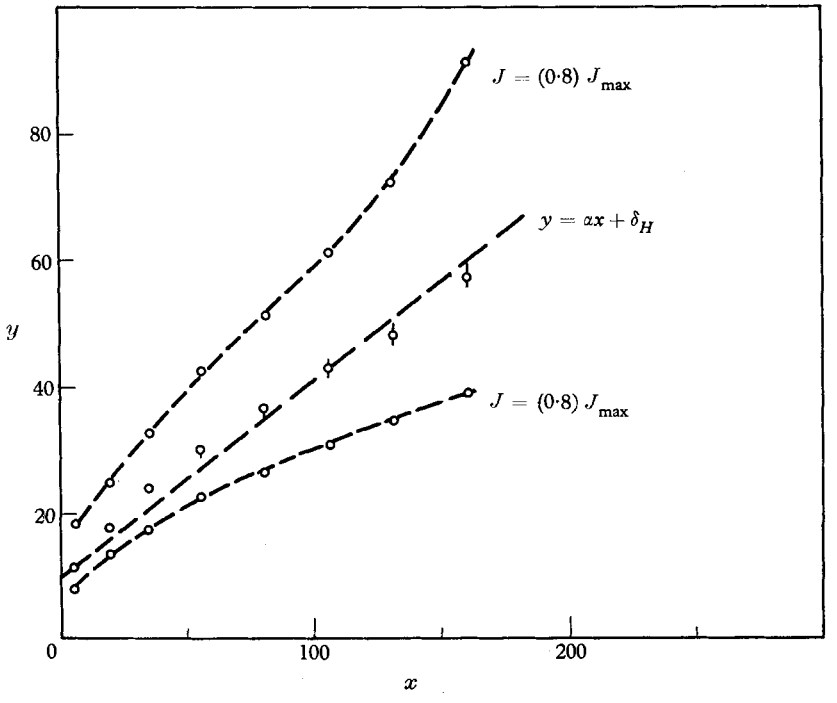

FIGURE 14. Location of maximum positive current, case 2–2: vertical lines at points are estimated uncertainty in location of maxima. Downstream boundary is at far right.

increase in velocity near the transverse boundary (case 3–2). The transverse velocity component, which is not shown, tends to increase upstream of the Alfvén line and decreases downstream of this line. Both of these effects are demonstrated by the change in location of the streamlines in cases 2–1 and 2–2, shown in figure 15.

Case	x	Decrease (%)	Increase (%)
1–3	357	1·4	1·0
1–4	357	8·4	3·9
2–2	131	5·8	4·9
3–2	357	9·2	2·5
4–2	131	4·6	3·7

TABLE 3. Maximum magnitudes of velocity changes from Hartmann flow values.

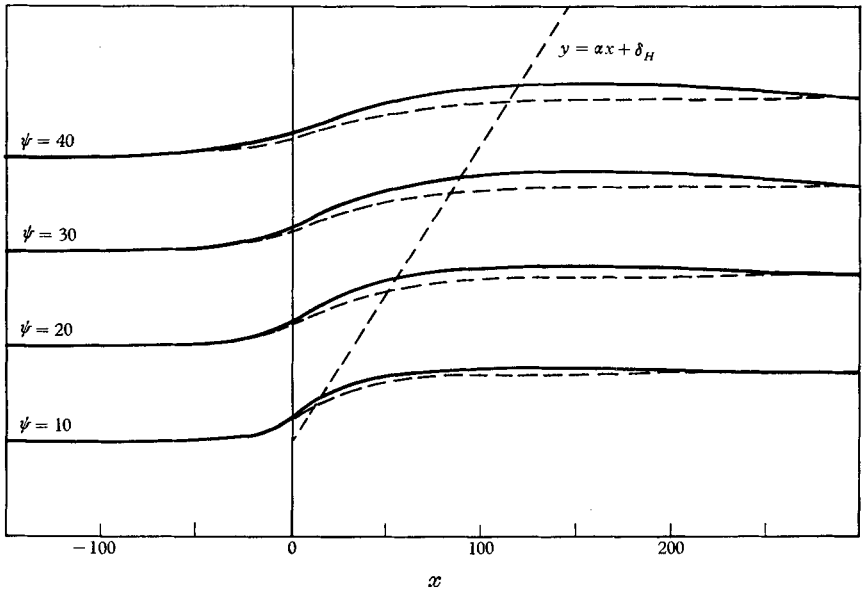

FIGURE 15. Location of streamlines for cases 2–1 and 2–2: broken lines are location of streamlines for case 2–1 (Hartmann flow). Downstream boundary is at far right.

It is further noted that the potential flow effect indicated by the maxima in velocity profiles in case 1–1 (Hartmann flow) completely disappears in case 1–4 (figure 10). However, in case 3–2 (figure 11), which is identical with case 1–4 with the exception of the position of the transverse boundary, the maxima reappear, indicating the potential flow effect, at a much greater distance from the plate (on the free stream side of the Alfvén line).

The normal component of the magnetic intensity at the plate is plotted in figures 16 and 17. It is seen that the changes in this component do not become appreciable until $\epsilon = 10^{-2}$ and the maximum amount is in case 3–2, figure 16. The normal component at the transverse boundary, not shown, tends to decrease from the applied value; this effect is attributed to the presence of the transverse

boundary. It is also of interest to compare the change in the normal component of magnetic field at the plate with that predicted by the linearized solution (equation (3.15)). The comparison of the maximum change is reflected in table 4.

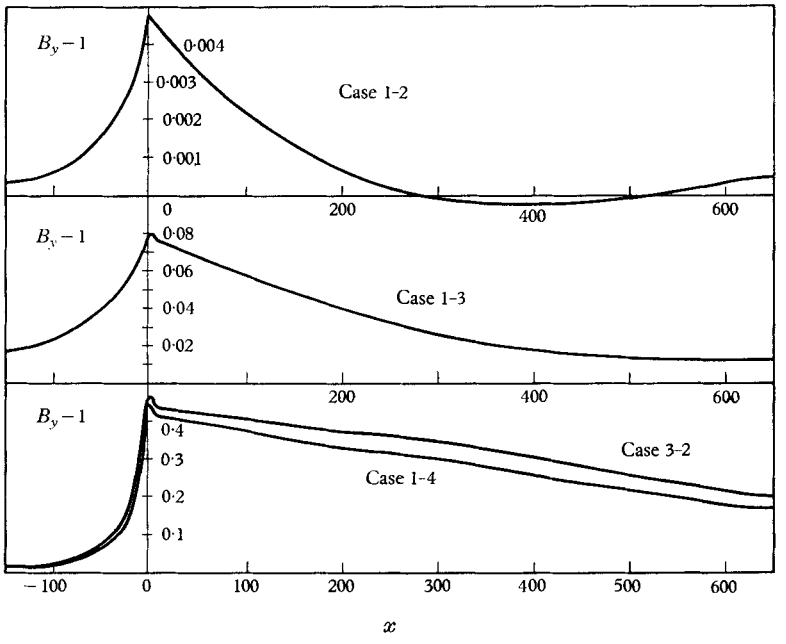

FIGURE 16. Normal component of magnetic field at plate, cases 1–2, 1–3, 1–4, 3–2.

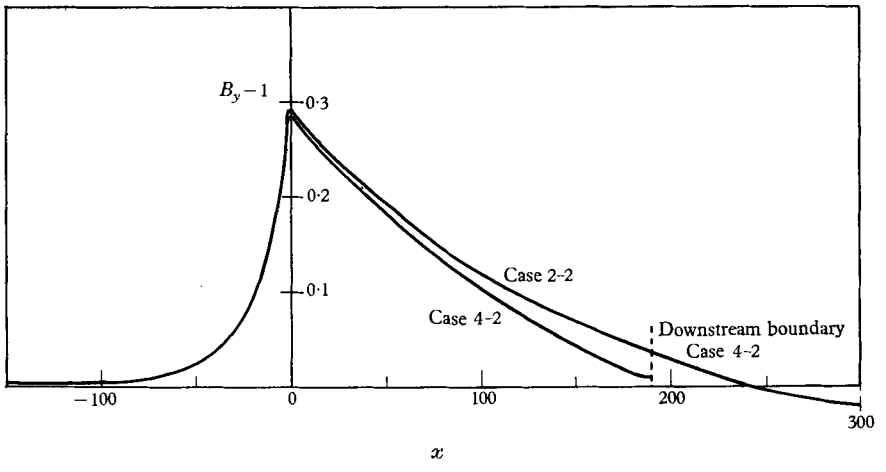

FIGURE 17. Normal component of magnetic field at plate, cases 2–2 and 4–2: downstream boundary for case 2–2 is located at $x = 300$.

Although the correlation is poor, the general character and order of magnitudes of the two results compare favourably. The rate of decay of this change is more rapid in the numerical results obtained than that predicted by the linearized solution.

The skin friction at the plate, tabulated in table 1, indicates that as the parameter ϵ is increased, the skin friction tends to decrease very slightly.

The preceding discussion can be summarized as follows: the presence of a non-conducting flat plate in an initially uniform, current-free flow of a conducting fluid in the presence of an applied transverse magnetic field, in addition to causing the formation of a thin viscous layer adjacent to the plate, excites an Alfvén-type disturbance which propagates into the free stream. This disturbance is readily identified as a region of high current density. The line of course has a finite width, which increases as $\sqrt{x}$ by diffusive effects. In addition to being a

	$(B_y - 1)/\epsilon^{\frac{1}{2}}$	
Case	Numerical	Equation (86)
1–2	0·150	0·87
1–3	0·794	1·195
2–2	0·920	0·995

TABLE 4. Comparison of magnetic field distortion as obtained from numerical and linearized solution.

region of high current density, the line tends to decrease the longitudinal component of velocity of the fluid as the fluid crosses it; the net result is the creation of a sizeable disturbance to the uniform flow. The position of the line is a strong function of the ratio of the Alfvén speed to the free-stream velocity (the parameter α), while the magnitude of the disturbance created is a strong function of the ratio of the two diffusivities ($\epsilon = \sigma\mu_0\nu$) and does not appear to become appreciable until $\epsilon > 10^{-2}$. This disturbance resulting from the Alfvén line is in marked contrast to the disturbance caused by a flat plate in the pure fluid mechanics case as it indicates that in flows of high electrical conductivity the effects of viscosity are no longer confined to a thin layer near the plate.

5.3. *Interpretation of general character of numerical results*

The general character of the numerical results suggests a flow field of the type shown in figure 4, which was constructed by analogy with the Rayleigh problem (see § 2.3); consequently, it is of interest to interpret these results employing the basic properties of Alfvén lines and viscous layers. In such an interpretation, it is helpful to recall the mathematical formulations governing the Rayleigh problem and the numerical problem differ in that (1) the former problem is linear, (2) the solutions to the Rayleigh problem exhibit damped wave characteristics in u and B, while the numerical problem exhibits damped wave characteristics in ζ and J, thus permitting potential flow-type solutions in u and B, (3) the relationship between the current density and field quantities is not analogous, and (4) the numerical problem contains effects due to finite boundary position.

Adopting as a tentative model the flow shown in figure 4, it is possible to derive, by methods completely analogous to those used for the Rayleigh problem in

§ 2.2, some approximate relations determining the flow conditions between the Alfvén line and the viscous layer. The approximation occurs due to the fact that the transverse velocities upstream and downstream of the Alfvén line cannot both be matched to that required by the viscous layer. One possibility is to require $v_1 = B_{x1} = 0$; the relations are then $u_2 = (1+\sqrt{\epsilon})^{-1}$, $B_{x2} = \sqrt{\epsilon}\,[\alpha(1+\sqrt{\epsilon})]^{-1}$, $v_2 = -(\epsilon\alpha^2)^{\frac{1}{2}}(1+\sqrt{\epsilon})^{-1}$, $\tan\theta = \alpha$, and $B_{y2} = (1+2\sqrt{\epsilon})(1+\sqrt{\epsilon})^{-1}$. It is evident that the results for u_2, B_{x2}, and $\tan\theta$ are analogous to those obtained from the Rayleigh problem. However, the fact that v_2 does not vanish prevents this solution from being entirely satisfactory. An alternative possibility is to require $v_2 = B_{x1} = 0$. This yields u_2 and B_{x2} as before, and $v_1 = (\epsilon\alpha^2)^{\frac{1}{2}}$, $\tan\theta = \alpha(1+\sqrt{\epsilon})$, $B_{y2} = (1+\sqrt{\epsilon})^{-1}$. Here again, the fact that v_1 does not vanish makes this solution unsatisfactory. To reconcile either of these solutions with the problem at hand, it is necessary to admit potential solutions for the velocity field. In a qualitative way, then, the complete solution will consist of a wave solution of the general type of either of the preceding ones, plus a potential solution in V and if necessary, B, in order that the boundary conditions may be satisfied. Further, it is not difficult to see that this potential flow must resemble the perturbation from uniform flow caused by a wedge of included half-angle $\beta = \tan^{-1}(\epsilon\alpha^2)^{\frac{1}{2}}$. This potential flow effect is evident in the velocity profile shown in figure 11. This fact at once makes the existence of some ultimate state (as defined for the Rayleigh problem) extremely problematical and at the same time permits amplification of the general conclusions regarding the nature of the flow.

These amplifications are limited in scope to that region of the flow where the superposition of the wave solution and the potential solution is valid, that is, the Alfvén line must be separated from the viscous layer, the parameter $\epsilon\alpha^2$ must be small in order that the transverse component of velocity induced by the Alfvén line is not large, and x must be limited such that the potential solution does not become dominant. With these restrictions, it may first be concluded that the slope of the Alfvén line is not constant and is somewhat greater than α based on the free-stream conditions at every point. This is evident from the fact that the wave solution must lie between the two presented previously. This conclusion is further supported by the character of the Alfvén line near the leading edge of the plate in the numerical results presented (figures 13 and 14), since the potential solution around the leading edge excited by viscous layer development is similar to the potential solution excited by the Alfvén line. Secondly, it may be concluded that the change in the longitudinal component of velocity across the Alfvén line is not as great as expected from the idealized wave solution due to the potential flow effect. These conclusions are certainly supported by the numerical results presented, although some consideration must be given to boundary effects, discussed in a subsequent paragraph, and the fact that cases 1–1 through 1–4 and 3–1, 3–2 allow only marginal separation of the Alfvén line and viscous layer.

It is further noted that the fully developed viscous layers of the Rayleigh and numerical problems are fundamentally different. The skin friction in the latter case is given by $(\partial u/\partial y)_{y=0} = \alpha\sqrt{\epsilon}\,u_2 B_{y2}$. From the wave-type solutions presented previously, it can be deduced that either $u_2 B_{y2} = (1+2\sqrt{\epsilon})(1+\sqrt{\epsilon})^{-2}$ or

$u_2 B_{y2} = 1$. Hence, it is expected that the skin friction change due to a change in ϵ, with $\epsilon\alpha^2$ fixed, is small for $\epsilon < 1$; this conclusion is supported by the data presented in table 1. The skin friction in the Rayleigh problem, however, is proportional to $1/(1+\sqrt{\epsilon})$. The difference may be attributed to the lack of analogy between the current density-field relationships of the two problems.

To complete the interpretation of the numerical results, some consideration must be given to the boundary effects. The effects of the upstream and downstream boundaries appear to be merely constraining ones, a fact which can readily be deduced in the latter instance by comparing the results previously presented for cases 2–2 and 4–2. The transverse boundary effect, indicated by comparing the results of cases 1–4 and 3–2, is primarily one of channelling the flow. The consequences of this effect may be deduced from the fact that if a transverse boundary is superimposed upon the elementary flow picture in figure 4, continuity considerations dictate that the velocity in front of the Alfvén line must increase from the unchannelled value. This effect is of the same qualitative nature as the potential flow effect previously discussed, and hence it causes the velocity behind the Alfvén line to be greater than the unchannelled value. As the significant parameter governing this effect is $\alpha l/h$, it is then expected that this effect is more pronounced for case 1–4 ($\alpha l/h = 0{\cdot}187$) than for case 3–2 ($\alpha l/h = 0{\cdot}079$); this conclusion is supported by the data in table 3. It is to be expected that this channelling effect tends to obscure the potential flow effect, a conclusion which is supported by comparison of figures 10 and 11. The increase in velocity due to channelling effects also tends to increase the current flow in the positive z-direction, which in turn tends to decrease the normal component of magnetic field. This effect is observed in the numerical results presented in figures 16–17 for the normal component at the plate, and was also observed in the behaviour of the normal component at the transverse boundary. Also, this effect undoubtedly plays an important part in the lack of correlation between the magnitudes of the distortion of magnetic field at the plate obtained numerically and those obtained from the linearized solution (see table 4). For at low values of ϵ ($< 10^{-2}$), the magnetic field distortion is small, and the effect of channelling due to the viscous layer on this distortion is comparable in magnitude to the distortion. Hence good correlation at these low values cannot be expected.

5.4. *Concluding remarks*

The most significant result of this work, apart from demonstrating feasibility of the numerical calculations, is the determination of the Alfvén wave-viscous layer disturbance created by the plate in a transverse magnetic field. Thus, for ϵ not small, the viscous effects are not confined solely to a boundary layer, but an appreciable free-stream disturbance is produced. This limits small disturbance analyses of the type performed by Sears & Resler (1959) to the case of $\epsilon \to 0$, as Stewartson (1960) has recently pointed out. When extended to the compressible case, this viscous layer-free stream interaction forecasts the formation of shock waves, which is an interesting experimental possibility if the necessary values of ϵ (~ 1) can be achieved.

In closing, the author expresses his appreciation to Profs. A. H. Shapiro and J. A. Shercliff for many valuable suggestions. This work was supported in part by the National Science Foundation, and in part by the U.S. Army (Signal Corps), the U.S. Air Force (Office of Scientific Research, Air Research and Development Command), and the U.S. Navy (Office of Naval Research). The facilities of the Massachusetts Institute of Technology Computation Center were used for the numerical calculations. A more detailed presentation of the work described in this paper can be found in an unpublished report by the author (Dix 1962).

REFERENCES

Bryson, A. E. & Rościszewski, J. 1962 *Phys. Fluids*, **5**, 175.

Carrier, G. F. 1959 *J. Appl. Phys.* **30**, 1769.

Carrier, G. F. & Greenspan, H. P. 1960 *J. Fluid Mech.* **7**, 22.

Chang, C. C. & Yen, J. T. 1959 *Phys. Fluids*, **2**, 393.

Dix, D. M. 1962 *Research Laboratory of Electronics, Tech. Rep.* 397, Massachusetts Institute of Technology.

Dix, D. M. & Cooper, L. Y. 1960 *Quarterly Progress Report, Research Laboratory of Electronics*, Massachusetts Institute of Technology.

Greenspan, H. P. & Carrier, G. F. 1959 *J. Fluid Mech.* **6**, 77.

Ludford, G. S. S. 1959 *Arch. Rat. Mech. Anal.* **13**, 14.

Moffatt, W. C. 1961 *Magnetogasdynamics Laboratory Rep.* no. 61–4, Massachusetts Institute of Technology.

Rossow, V. J. 1960 *Phys. Fluids*, **3**, 395.

Sears, W. R. & Resler, E. L. 1959 *J. Fluid Mech.* **5**, 257.

Stewartson, K. 1960 *J. Fluid Mech.* **8**, 82.